Icarus **160**, 350–358 (2002)
doi:10.1006/icar.2002.6967

The Composition of Saturn's Rings

F. Poulet and J. N. Cuzzi

NASA Ames Research Center, MS 245/3, Moffett Field, California 94035
E-mail: poulet@despace.obspm.fr

Received June 29, 2001; revised July 3, 2002

A composite spectrum between 0.30 and 4.05 μm of Saturn's rings is analyzed using the Shkuratov scattering theory (Shkuratov *et al.* 1999, *Icarus* 137, 235–246). Several types of surface and composition are discussed. We demonstrate that both the strong reddening over the interval 0.3–0.7 μm and the water ice absorption features are well reproduced by an intimate ("salt-and-pepper") mixture of four coarse particles of two different materials: 93% are grains (typical sizes of 10, 200, and 2000 μm) of water ice containing a few percent of refractory organic solid (tholin) impurities within their bulk, and 7% are coarse grains of a dark material (amorphous carbon). The cosmogenic implications of the inferred composition are discussed.

Key Words: **planetary rings, Saturn; spectroscopy; surfaces, planets.**

1. INTRODUCTION

The composition of Saturn's rings, which is a critical constraint on their origin and evolution, is a well-known problem: water ice is the only molecule detected, although many spectral characteristics indicate the presence of other unidentified substances. Here, we suggest a possible composition from the modeling of a composite spectrum in the UV/near-infrared range.

Water ice has long been accepted as the most prominenting component based on a combination of near-infrared and microwave observations (Pilcher *et al.* 1970, Clark and McCord 1980, Epstein *et al.* 1984). Different investigations directed at different bands have led to different grain size results. The ice bands in the near-infrared were fit by regolith grains of about 200 μm diameter (Pollack *et al.* 1973, Clark 1980). More recently, Alix (1998) reinvestigated the spectrum analyzed by Clark (1980). The near-infrared spectrum and also the position of the H_2O absorption wall between 0.165 and 0.17 μm can be reproduced by particles of about 40 μm diameter. However, water ice is certainly not the only constituent of the rings. The particle visible albedos (0.15–0.20 for C ring and Cassini division particles, and 0.4–0.6 for A and B ring particles) are much too low for impurity-free water ice. Furthermore, the rings are distinctly red between 0.3 and 0.7 μm, and there are hints of a weak absorption near 0.85 μm in data averaged over the entire ring system from Clark and McCord (1980) and Karkoschka (1994). These properties require the presence of some nonicy, probably nonvolatile constituents. Because there are no absorption features detected in the near-infrared range other than those of water ice, the identification of the nonicy substance(s) can be attempted on the basis of the reddening characteristic alone. Cuzzi and Estrada (1998) showed that the color of rings could be best modeled by a small amount of a reddish absorber such as organic solids. However, this study was limited to three *Voyager* broad filters (UV, V, G), so the composition of the rings has still never been studied in a wider spectral range. Moreover, the possible discrete absorption in the 0.85-μm range, usually attributed to certain silicates containing Fe^{3+}, was also never reproduced.

To help address such questions, we have tried to determine the composition of Saturn's rings by modeling a composite spectrum between 0.3- and 4.05-μm wavelength with the Shkuratov albedo model (Shkuratov *et al.* 1999). In the next sections, we describe the construction of the composite spectrum (Section 2), discuss the choice of the scattering model (Sections 3.1 and 3.3) and end-members (Section 3.2), compare the results of the models to the data (Section 3.4), and discuss the cosmogenic implications of the results (Section 4).

2. A COMPOSITE SPECTRUM

To date, the composite spectrum (0.33–4.05 μm) published by Clark and McCord (1980) has been the reference spectrum of Saturn's rings. This spectrum consists of a combination of three data sets: (1) the Lebofsky and Fegley (1976) data set giving the reflectance between 0.33 and 0.65 μm, (2) the measurements by Clark (1980) covering the spectral region 0.65 to 2.5 μm, and (3) the Puetter and Russel (1977) spectrum between 2.8 and 4.05 μm. These three spectra have been combined and scaled to unity at 1.02 μm by Clark (1980). Molina *et al.* (1995) obtained spectra without absolute calibration in the 1.4- to 2.4-μm and 2.8- to 4.5-μm ranges whose shapes agree with those of Clark and McCord (1980). Karkoschka (1994) obtained a ground-based spectrum in the visible range whose absolute calibration and spectral resolution were better than those of the Lebofsky and Fegley (1976) and the Clark and McCord (1980) spectra. So, we combined the Karkoschka spectrum with the rest of the composite spectrum presented by Clark and McCord

0019-1035/02 $35.00

(1980). Then, we scaled the whole spectrum at 0.94 μm to the value of 0.46, the albedo given by the Karkoschka spectrum. The composite spectrum is shown in Fig. 2. We ignore all angle dependences of reflectance, which can affect the spectrum to some degree (Cuzzi *et al.* 2002, Poulet *et al.* 2002a).

3. MODEL FITTING

3.1. Choice of the Scattering Model

The spectrum of Saturn's rings in the UV/near-IR range resembles those of the higher albedo satellites of Saturn (Cruikshank *et al.* 1999). These spectra are characterized by a significant reddening at visible wavelengths, which is among the largest reddenings of the Solar System objects (see Fig. 7 of Poulet *et al.* 1999), and a blue-neutral continuum slope in the 1.4- to 2.5-μm region combined with strong water ice absorption bands.

Silicates and organics are usually considered to produce a red slope in the visible spectrum. Previous modeling of the reddening of objects such as Saturn's satellites Rhea and Iapetus and some Centaurs (Asbolus and Pholus) with the widely used Hapke theory (Hapke 1993) or its derivatives gave suspect results in terms of the derived grain sizes of some constituents, which were smaller than the wavelength (T. Roush and C. Dalle Ore, personal communications, Cruikshank *et al.* 1998a, Barucci *et al.* 2000, Owen *et al.* 2001). These results violate key assumptions of geometrical optics in the Hapke theory used by these authors.

The blue slope of the continuum, typical of pure, particulate water ice, is mainly due to the increasing strength of its combination and overtone bands as the wavelength increases. If the water is mixed with dark material, the continuum reflectance of the mixture increasingly approaches that of the dark material as its abundance is increased (Clark 1981, Clark and Lucey 1984). Thus, the continuum reflectance of a water-ice/dark-material mixture can have a wide range of slopes depending on the coloring agent, its concentration, and the size of grains (Section 3.4). The Hapke scattering theory fails to reproduce the blue continuum observed in the spectra of several of Saturn's satellites (Benedix *et al.* 1998). Grundy *et al.* (1999) pointed out that another component was required to achieve the blue slope. Eventually, Brown *et al.* (1999) introduced a dark blue (but unknown) material to match the blue continuum reflectance of Nereid.

We choose to use the spectral albedo model developed by Shkuratov *et al.* (1999) for fitting the characteristics of the UV/near-IR spectrum of Saturn's rings. This geometrical optics model, based on the equivalent-slab approximation for calculating the albedo of a particle, provides the spectral geometric albedo of a powdered surface. The light scattering at wavelength λ from a particulate surface of a material with real and imaginary parts of the refractive index n and k is described by two parameters: (1) the ray propagation between scattering points, characterized by the optical depth $\tau = 4\pi kl/\lambda$, where the parameter l is the average length of light propagation in a particle between internal reflections (for transparent particles, l should be equal approximately to the average diameter of the particle), and (2) the coefficient P, which is the porosity of a regolith-covered surface. We take a value of $P = 0.9$, which should be typical for the regolith of Saturn's ring particles (Poulet *et al.* 2002a); in any case, Shkuratov *et al.* (1999) showed that the porosity does not significantly affect the albedo of bright particulate surfaces.

Shkuratov *et al.* (1999) considered two types of particulate mixtures. The first model (called here model 1) is a mixture of coarse particles of size much larger than λ. In a sense, this model is similar to an intimate (or "salt-and-pepper") mixture. The second model (model 2) consists of coarse particles still $\gg\lambda$ in size with fine absorbing independent inclusions of size $\ll\lambda$ which do not affect the real index of refraction n, but increase the imaginary index k. This model belongs to the type of models defining an "intra" or "molecular" mixing of constituents. From models 1 and 2, we constructed a third model (model 3) in which particles of different intramixtures are intimately mixed.

3.2. Choice of the Optical Constants and End-members

We select the surface composition of Saturn's ring particles by trying to satisfy the following observational constraints:

1. the red slope from 0.3 to 0.7 μm,
2. the shape and the depth of water ice absorption at 1.5 and 2.0 μm,
3. the shape of the bump at 3.5 μm, and
4. the correct albedo (0.47 at 0.8 μm).

The data analyzed here do not have adequate precision to distinguish clearly between the crystalline and amorphous phases of water ice. However, we recently obtained new spectroscopic data for the rings with the NASA Infra-Red Telescope Facilities (Mauna Kea) which reveal a strong absorption band at 1.65 μm typical of the crystalline water ice (Poulet *et al.*, in preparation). So, the values of optical constants for H_2O ice are taken from Grundy and Schmitt (1998) between 1.0 and 2.7 μm ($T = 80$ K) and from Hudgins *et al.* (1993) beyond 2.7 μm ($T = 100$ K). Because the optical constants for amorphous or crystalline water ice are not available in the UV/visible range, we adopted the values from Warren (1984) between 0.3 and 1.0 μm at $T = 270$ K.

The spectrally low albedo amorphous carbon (Rouleau and Martin 1991) is also included in the scattering calculations. This constituent is a standard to lower the average spectral reflectance. Note that its spectral neutrality means that carbon alone will not have an effect on the red slope and the blue slope of the continuum.

We need additional components to produce the observed red slope in the UV/visible range. The frustrating lack of diagnostic features other than those due to water ice makes the choice of such red component(s) difficult. Silicates and organics, both possible candidates, are usually considered. Some of these candidates in interplanetary dust survive the atmospheric entry to Earth, and we similarly expect some of the components to survive emplacement (or exposure) on ring particles. Therefore, there should be a huge variety of compounds to work with.

Actually (and unfortunately), the variety is limited. The major limitation comes from the small number of materials whose optical constants have been determined over the range of wavelength studied here. Among the reddish substances, we only found a few minerals (a few data sets of olivine and pyroxene) and some so-called tholins, or organics produced by plasma irradation of organic-rich gases.

The real and imaginary indices of refraction of various reddish materials are from a variety of sources. The optical constants of olivine come from Mukai and Koike (1990) and Pollack *et al.* (1994). Those of pyroxene are given by Pollack *et al.* (1994). We examined Titan tholin made from irradiation of a gas mixture of $N_2 + CH_4 = 0.9 + 0.1$ (Khare *et al.* 1984) and Triton tholin made from a 99.9 : 0.1 mixture of $N_2 : CH_4$ gases (Thompson *et al.* 1989). We also used a solid residue produced by irradiation of a solid created from a gas mixture of $H_2O : CH_3OH : CO_2 : C_2H_6$ in the following proportions 100 : 20 : 4 : 1 (B. N. Khare, unpublished data, referred to as ice tholin in the following).

R. N. Clark (1999, personal communication) indicates a continuing belief in the reality of the 0.85-μm feature. But he suspected that it might be weaker than apparent in the Clark and McCord (1980) spectrum, as the Karkoschka (1994) spectrum that we analyze here supports. Cuzzi *et al.* (2002) attempted (unsuccessfully) to confirm the reality of this absorption using HST broadband photometry to search for spatial variations in its strength. Although this absorption is still not certain, we attempted to satisfy its shape and its depth, to constrain the maximal amount of Fe^{3+} mineral. Iron oxides and iron-bearing sulphates provide strong candidates for the cause of this absorption. Unfortunately, the optical constants of such materials do not exist. We derived information on the optical properties from laboratory spectra by using the Shkuratov model (Shkuratov *et al.* 1999): the imaginary index fraction $k(\lambda)$ can be found if the spectral albedo $A(\lambda)$ is known and if estimates for the parameters n, l, and P described previously are available. From the spectral library of USGS (Clark 1993), we extracted the optical constants of several iron oxides (samples of hematite and of goethite) and iron-bearing sulphates (samples of jarosite) which show strong absorption near 0.85 μm.

To select the possible candidates, we compare the reddening of water ice particles contaminated by small inclusions of either the mineral or organic compounds already discussed above with the reddening of ring particles (Fig. 1). Water ice/mineral intramixtures do not satisfy the spectral shape: they are too steep in the UV range and too flat beyond 0.4 μm. Moreover, the prominent silicate spectral feature at 0.9–1.1 μm is very strong with only a very small amount of silicate. So, we believe that reddish silicates can probably be ruled out by a combination of the shape of the red slope and the lack of significant absorption in the 0.9- to 1.1-μm region (see also Cuzzi and Estrada 1998). Of these several iron-bearing compounds, only iron-bearing sulphate jarosite could provide a good match to the reddening of rings. In future analyses, this constituent will be considered (Section 3.4).

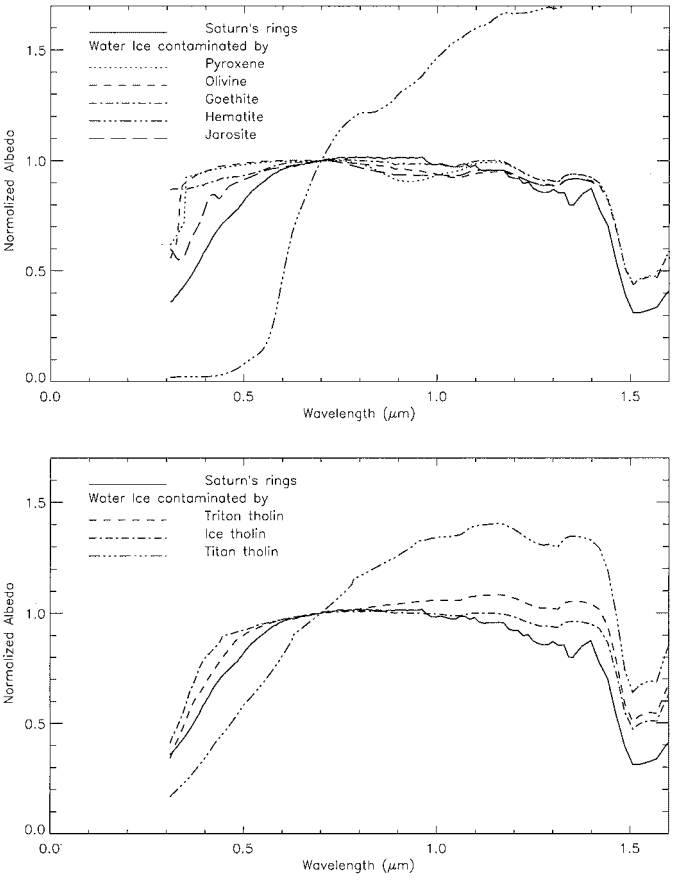

FIG. 1. (Upper panel) Comparison between the reddenings of Saturn's rings and synthetic spectra of water ice particles contaminated as an intramixture by different minerals (olivine, pyroxene, iron oxides goethite and hematite, and iron-bearing sulfate jarosite) in a proportion of 1% by volume. (Lower panel) Comparison between the reddenings of Saturn's rings and synthetic spectra of water ice particles contaminated as an intramixture by different organic compounds in a proportion of 1% by volume.

By contrast, the organic compounds match the slope of Saturn's rings in a satisfactory way. Note that not all organic materials provide an acceptable fit. The Titan tholin/water ice mixture exhibits too steep a spectral slope. Nevertheless, it leads us to consider a mixture of this material with other less red organic or jarosite material as a possible solution (Section 3.4).

Obviously, our procedure for selecting end-members is somewhat arbitrary. Matching a slope is not a satisfying approach for proving a surface composition. It is suited for proving that something is not present, but it is not so good for proving that something is here. However, since the tholins provide a far better fit than reddish silicates, we believe that they likely are the best reddish candidates (of any known materials).

3.3. Choice of the End-type of Surface

Three types of surface (model 1: intimate mixture, model 2: intra-mixture, and model 3: a combination) were investigated. The best fits to the data were found by a manual iterative

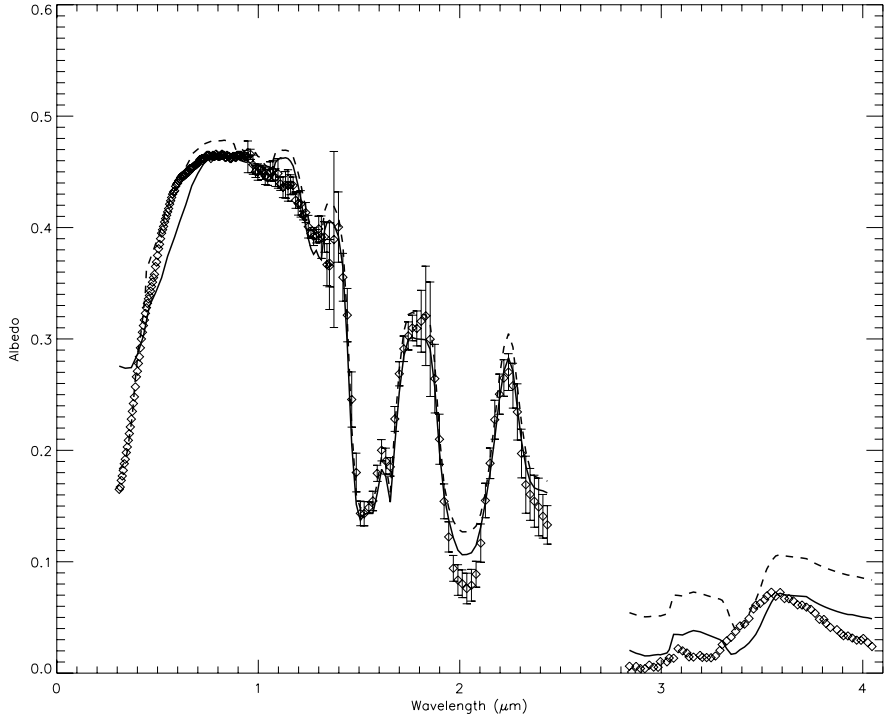

FIG. 2. The composite spectrum (diamonds) and two synthetic spectra using model 1 (called intimate mixture). One model (solid line) is an intimate mixture of 80% pure water ice (20- and 700-μm grain sizes) and 20% organic compound (Titan tholin and ice tholin, 10-μm grain size). If we relax the constraint of the geometrical optics for the reddish tholins and assume a grain size of 2 μm, a better fit to the reddening is obtained (dashed line), but the model still fails to reproduce the near-infrared part.

technique in which the principal effects of each component were first evaluated individually and then combined. When a rough solution emerges, a downhill simplex technique was used to minimize the RMS residual.

Model 1 (coarse particles of different compositions intimately mixed; thin line in Fig. 2) fails to reproduce the spectrum. In particular, the very large proportion of tholin (about 20%) necessary for achieving the red slope introduces a strong brightness beyond 2.8 μm and an absorption band at 3.4 μm. We explored a range of values for grain sizes and abundances, but no satisfactory combination has been found. For these tests, the grain sizes of all the components are much larger than the wavelength. If we relax this condition for the red organic absorber, we found a better fit of the reddening, as expected (dashed line in Fig. 2). Making the tholin grains smaller allows light to leave the regolith with fewer internal scatterings inside grains, and thus with less absorption. This leads to an increase in the color of the material (see Fig. 4 of Poulet *et al.* 2002b). However, the large proportion of organic compound required for the fit of the reddening still introduces a strong brightness beyond 2.8 μm and a typical absorption band at 3.4 μm.

The model 2 best fit (thin line in Fig. 3) is a surface composed of water ice particles of three different grain sizes (10, 170, and 1300 μm) containing fine inclusions of amorphous carbon and ice tholin in a small proportion by volume (respectively 0.3 and 4%). It is impossible to match both the reddening and the level of albedo between 0.7 and 1.5 μm. We can better adjust the reddening (dashed line in Fig. 3), but if we do so, the albedo is no longer well fitted.

These experiments with the models 1 and 2 can be interpreted as following. First, the only way to reproduce the reddening is to incorporate a red contaminant (organic compounds here) as small inclusions in the bulk of coarse water ice particles (called here intramixing of constituents). The second experiment indicates that spectrally neutral amorphous carbon, which nicely accounts for the level albedo constraint, can be mixed with water ice particle as an intimate mixture only. Consequently, a solution begins to emerge: to consider a third type of surface (Section 3.1) with the red contaminant(s) intramixed with water ice and the dark component intimately mixed.

3.4. Results

Single H_2O ice grain size. Two-component intimate mixtures (dark water ice and amorphous carbon) were calculated as a function of variations in both the relative abundance and the grain size of each component. To achieve the correct albedo level in the 0.7- to 1.0-μm region, a relative abundance of about 7% is required for the amorphous carbon. We cannot constrain the diameter l of carbon particles, because no absorption band exists. A lower limit can be given only, as explained in the following. For $l > 1$ μm, the internal-transmission factor $\exp(-\frac{4\pi kl}{\lambda})$,

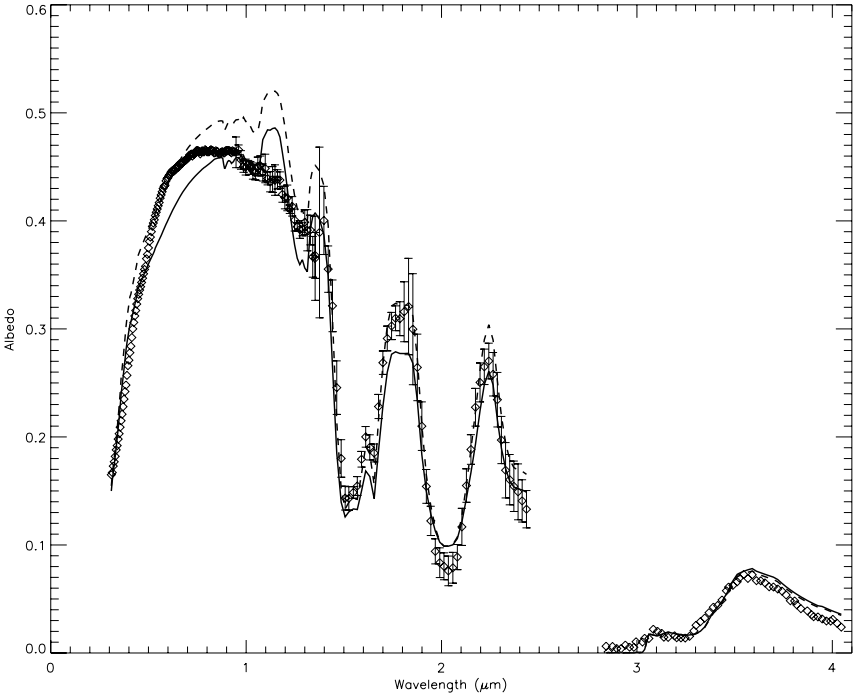

FIG. 3. The composite spectrum (diamonds) and two synthetic spectra using model 2 (called molecular mixture or intra mixture). The two models are made of water ice grains contaminated by ice tholin and amorphous carbon inclusions in different proportions (see Section 3.3).

which defines the total fraction of light entering the particle that reaches another surface after one transit, is near zero. Since geometrical optics also requires l larger than λ, all values l larger than 10 μm are compatible with a concentration of carbon particles of 7%. Figure 4 illustrates the calculations for intimate mixtures of amorphous carbon/water ice contaminated by tholin inclusions for H_2O ice grain diameter of 20, 100, and 1000 μm, respectively. As can be seen, the synthetic spectra show a strong

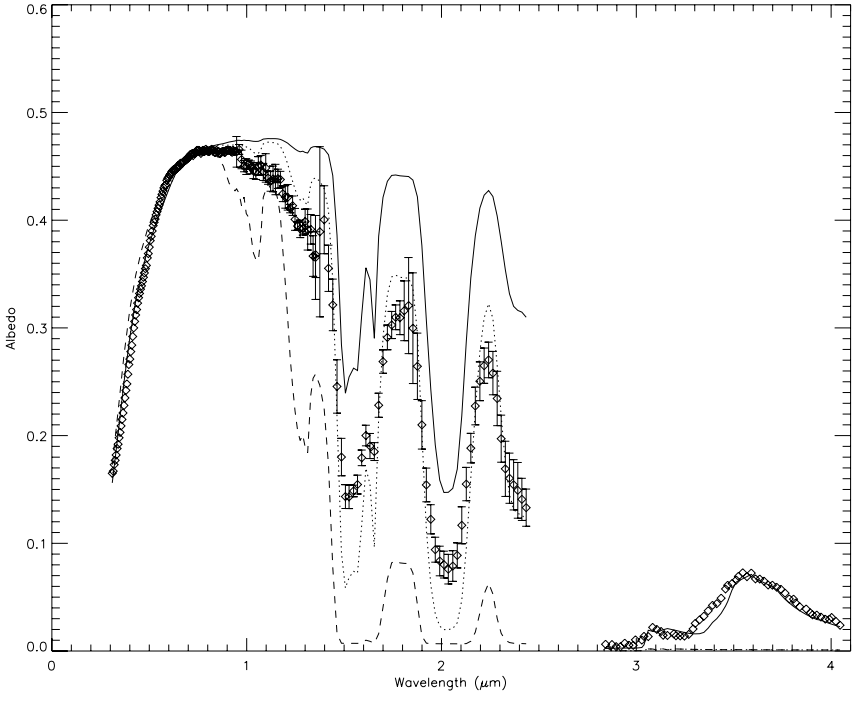

FIG. 4. The composite spectrum (diamonds) and three synthetic spectra made of a two-component intimate mixture of amorphous carbon grains (relative abundance 7%, grain size 10 μm) and water ice grains contaminated by organic compounds. The size of the water ice grains is equal to 20 μm (thin line), 100 μm (dotted line), and 1000 μm (dashed line).

sensitivity to the H_2O grain size. The spectrum beyond 3.0 μm is well reproduced with a grain size of 20 μm, but the slope of the continuum in the 1.0 and 2.5 μm is not blue enough. By contrast, the mixture with 100-μm grain size has a satisfactory slope for the continuum but water ice absorptions that are too strong. Recall that all the water ice grains are contaminated by organic compound inclusions (ice tholin and Titan tholin here). The proportion by volume of red contaminants required to reproduce the visible reddening depends on the size of water ice grain (from about 0.7% for the 20-μm grains to 0.015% for the 1000-μm grains). These calculations show that a single typical water ice grain size cannot alone reproduce all the near-infrared characteristics of the spectrum. Therefore, we need to include several different mixed H_2O ice grain sizes.

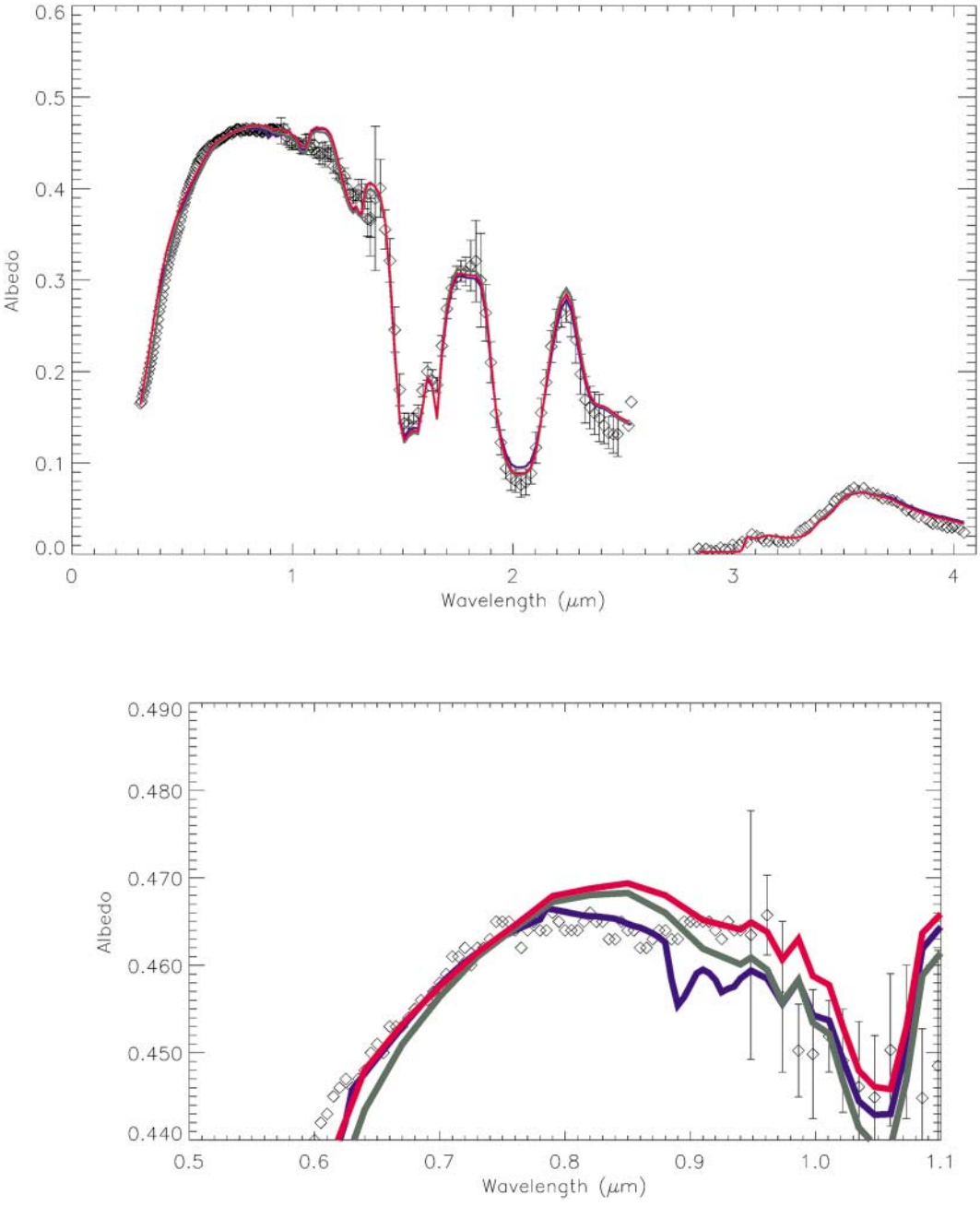

FIG. 5. (Upper panel) A set of three synthetic spectra using model 3 (blue line: four-component intimate mixture of water ice grains contaminated by ice tholin and jarosite inclusions, amorphous carbon, and pure water ice grains of two sizes; green line: four-component intimate mixture of 200-μm water ice grains contaminated by ice and Titan tholin inclusions, amorphous carbon, and pure water ice grains of two sizes (10 and 2000 μm); red line (best fit): four-component intimate mixture of 10-μm water ice grains contaminated by ice and Titan tholin inclusions ($2.8 \pm 0.8\%$), amorphous carbon ($7 \pm 0.5\%$), and pure water ice grains of two sizes (200 μm, 28% and 2000 μm, 7%). (Bottom panel) Detail of the 0.85-μm region.

Mixed H_2O ice grain sizes. Several-component intimate mixtures (a single amorphous carbon grain size, and mixed H_2O ice grain sizes) were calculated as a function of variations in both the relative abundance and the grain size of each component. Water ice grains of three sizes (typically 10, 100, and 1000 μm) intimately mixed with amorphous carbon grains are required to give a good fit of the near-infrared features of the spectrum. The best fit (RMS ~ 0.028) of the entire spectrum is obtained with an intimate mixture of four components (red line in Fig. 5): 55% H_2O ice grains (diameter of 10 μm) containing 3.6% per volume of ice tholin and Titan tholin inclusions, 30% pure H_2O ice grains with grain size 170 μm, 8% pure H_2O ice grains with grain size 2000 μm, and 7% amorphous carbon. The quantity of organic material is larger than the value of 0.35% derived by Cuzzi and Estrada (1998), who calculated the effective grain refractive indices using the Maxwell–Garnett theory but assumed that all water ice grains had the same fraction of organics. We find that different combinations between two organic compounds (among those considered, i.e., Titan tholin, ice tholin, and Triton tholin) intramixed with the 10-μm water ice grain can fairly reproduce the red slope. This quantity depends on the size of the water ice grain. We then constructed a satisfactory model with RMS ~ 0.027 (green line in Fig. 5) by introducing the inclusions of organic compounds in the larger H_2O ice grains. In this case, 0.12% of organic contaminant inclusions in the 200-μm water ice grain is required; all the other relative abundances and grain sizes remain similar to those of the best fit: 55% (resp. 5%) of pure water ice grains with 10 μm (resp. 4000 μm) size and 6% of amorphous carbon grains. This result indicates that the tholin inclusions could be found in all water ice grains of all sizes. However, it is numerically difficult to find a solution where tholins could be included in the water ice grains of each typical size (10, 200, and 2000 μm), because it would give 12 new parameters to fit (instead 8), increasing considerably the computing time.

Although the best models (red and green lines) give a fair fit, two regions show notable mismatches. The first is between 1.1 and 1.3 μm. This discrepancy could be related to the size of water ice grains: the bigger the grain, the stronger the drops in reflectance between 1.1 and 1.4 μm. It is unclear what the true sense of these discrepancies is; they could be due to a difference in the actual optical constants of the water in the ring particles versus those measured in the laboratory or they could be due to poor quality data (R. Clark, 1999, personal communication). The second mismatch is found at 0.85 μm, which could correspond to the Fe^{3+} presence (Section 3.2). The blue line of Fig. 5 illustrates a calculation with the same kind of mixture as the red line fit, except that we replaced ice tholin by jarosite. In this case, the fit is similar to the best fit (RMS = 0.027). However, there is a significant discrepancy in the UV region due to an absorption of jarosite, absorption which was never reported. We dismiss the presence of iron-bearing sulfate, so the modeling of this absorption remains an issue.

The abundance of the coarse-grained carbonaceous material is constrained by the level of the albedo in the 0.7- to 1.0-μm region. The errors on the flux correspond to an uncertainty of about $\pm 0.5\%$ on the relative abundance. Because it is simply a useful stand-in of the nature of the dark material, we considered other unknown materials by changing the complex refractive indices of the amorphous carbon by $\pm 50\%$. We then found proportions between 5 and 8%. The water ice grain sizes are well constrained by the albedo and the absorption bands. Exploration of a range of grain sizes and abundances around those selected for the best fit (red line in Fig. 5) gives an uncertainty of about 10%. The abundance of the organic component is constrained by the reddening in the UV/visible range. A change of $\pm 5\%$ in abundance results in a change of about $\pm 2\%$ of albedo. Estimated errors in the imaginary refractive indices of tholins are thought to be $\pm 30\%$ (Khare *et al.* 1984), which implies an error of $\pm 40\%$ on the proportion of organics.

4. DISCUSSION AND CONCLUSION

We assert in this paper that the Saturn's ring particles contain complex carbon compounds represented here by tholins and that a neutral dark material should be present as coarse particles segregated from the bulk water icy-tholin-jarosite material.

Organic molecules can be included in an icy regolith both by endogenic and exogenic processes (see, e.g., a detailed discussion in Cruikshank *et al.* 1998a). In summary, it is believed that the Solar System formed from interstellar dust which contained carbon and organic-rich material. Moreover, radiation by ultraviolet photons, solar wind particles, and galactic cosmic rays causes spectral changes of the organic material. These two basic sources of organic material could explain the strong evidence for organic solids on Pholus (Cruikshank *et al.* 1998a), Iapetus (Owen *et al.* 2001), and Ganymede, and Callisto (McCord *et al.* 1997) and the possible evidence on Triton and Pluto (Cruikshank *et al.* 1998b) and other reddish Kuiper Belt objects (Davis *et al.* 1998, Jewitt *et al.* 2000, Barucci *et al.* 2000, Poulet *et al.* 2002b). As suggested by Cuzzi and Estrada (1998), the similarity between the reddish, possibly organic-bearing intrinsic composition of the rings and Centaurs and some Kuiper Belt objects appears to favor the scenario of ring formation by tidal breakup of a heliocentric body whose small organic molecules had not been depleted of hydrogen by solar UV and heat. On the other hand, Owen *et al.* (2001) pointed out in their analysis of the surface composition of Iapetus that the organic material exhibits a ratio of nitrogen to carbon (N/C) much larger than the solar value. They suggest that the Iapetus dark material could come from an impact on Titan, where atmospheric photochemistry has been producing nitrogen-rich organic compounds.

While some organic absorber may color the water ice grains, we do not claim that we have identified it unambiguously in this work. We reiterate, however, that organic compounds could be abundant in the Solar System and we carry these absorbers because (a) their optical constants have been measured, which

is not the case for other potential materials such as numerous minerals, and (b) others have relied on them frequently to explain the reddish color in the outer Solar System.

The 0.85-μm feature is usually assumed to be due to the Fe^{3+} electronic transition. However, we found that the position and the depth of the band are not consistent with iron-bearing minerals or sulphates. We point out that new spectrocopic data are necessary to confirm or refute this absorption.

Amorphous or poorly graphitized carbon is the most abundant carbon-rich material in interplanetary dust particles (Owen *et al.* 2001). This dark material could come from meteoritic bombardment, as proposed by Cuzzi and Estrada (1998). Microwave observations obtained by Epstein *et al.* (1984) showed that the mass fraction of any nonicy *silicate* material in the A and B rings must be less than 10% if the material is uniformly distributed. Because the amorphous carbon has a higher absorption coefficient (about 5 cm^{-1} at 3 mm from Mennella *et al.* 1998) than silicate material (0.8 cm^{-1} from Epstein *et al.* 1984), we estimate from Eq. (1) of Epstein *et al.* (1984) that the amorphous-carbon/ice mass ratio should be less than a few percent if the materials are uniformly mixed. Our spectral modeling is consistent with a ring particle surface made of 7% carbonaceous material intimately mixed ("salt-and-peper" mixture) with the water ice material. It must be checked whether the model of Saturn's ring particles which we derived could emit too much in the microwave region.

Since the radiative transfer model presented here is now able to reproduce the general trend of the spectrum of the rings, new spectro-imaging observations should be analyzed to help determine the nature and the distribution of dark and red materials. Multicolor photometry of the rings from HST indicates that the ring system spectra in the UBVRI filters vary noticeably with region (Cuzzi *et al.* 2000). More recently, we obtained spatially resolved higher spectral resolution reflectivity measurements in the 0.9- to 5.0-μm region which should further improve our understanding of ring compositional variability and hopefully resolve the remaining discrepancies. This analysis will be presented in a future paper (Poulet *et al.*, in preparation).

ACKNOWLEDGMENTS

We thank Ted Roush for helpful conversations and for providing us with many refractive indices. We thank Ted Roush, Dale Cruikshank, and Cristina Dalle Ore for useful conversations on the colors of material in the Solar System and the current modeling of the spectra of some satellites of Saturn. This work was performed while FP held a National Research Council Resident Research Associateship (NASA Ames Research Center) and a San Jose State University Foundation grant, supported by NASA grants to JC and DC.

REFERENCES

Alix, J.-M. 1998. *Réflectivité et transmission des anneaux A et B de Saturne: Effets de la distribution de taille et nature physico-chimique des particules des anneaux.* Ph.D. dissertation, Université Paul Sabatier, Toulouse, France.

Barucci, M. A., C. de Bergh, J.-G. Cuby, A. Le Bras, B. Schmitt, and J. Romon 2000. Infrared spectroscopy of the Centaur 8405 Asbolus: First observations at ESO-VLT. *Astron. Astrophys.* **357**, L53–56.

Benedix, G. K., T. L. Roush, T. C. Owen, D. P. Cruikshank, T. R. Geballe, C. M. Dalle Ore, B. N. Khare, and C. de Bergh 1998. Surface composition models of the leading surfaces of Rhea and Dione. *Bull. Am. Astron. Soc.* **30**, 4409.

Brown, R. H., D. P. Cruikshank, Y. Pendleton, and G. J. Veeder 1999. Water ice on Nereid. *Icarus* **139**, 374–378.

Clark, R. N. 1980. Ganymede, Europa, Callisto, and Saturn's rings—Compositional analysis from reflectance spectroscopy. *Icarus* **44**, 388–409.

Clark, R. N. 1981. The spectral reflectance of water–mineral mixtures at low temperature. *J. Geophys. Res.* **86**, 3074–3086.

Clark, R. N. 1993. Spectroscopy of rocks and minerals and principles of spectroscopy. In *Manual of Remote Sensing* (A. Rencz, Ed.), Chapter I. Wiley, New York.

Clark, R. N., and P. G. Lucey 1984. Spectral properties of ice–particulate mixtures: Implications for remote sensing applications. *J. Geophys. Res.* **89**, 6341–6348.

Clark, R. N., and T. B. McCord 1980. The rings of Saturn–New near-infrared reflectance measurements and a 0.326–4.08 micron summary. *Icarus* **43**, 161–168.

Cruikshank, D. P., and 14 colleagues 1998a. The composition of Centaur 5145 Pholus. *Icarus* **135**, 389–407.

Cruikshank, D. P., T. L. Roush, T. C. Owen, E. Quirico, and C. de Bergh 1998b. The surface composition of Triton, Pluto, and Charon. In *Solar System Ices* (B. Schmitt, C. de Bergh, and M. Festou, Eds.) pp. 655–684. Kluwer, Dordrecht.

Cruikshank, D. P., T. L. Roush, T. C. Owen, T. R. Geballe, C. M. Dalle Ore, B. N. Khare, and C. de Bergh 1999. Saturn's icy satellites: Infrared reflectance spectra of Rhea, Tethys, Dione, and Iapetus at lambda >2.5 μm. *Bull. Am. Astron. Soc.* **31**, 302.

Cuzzi, J. N., and P. R. Estrada 1998. Compositional evolution of Saturn's rings due to meteoroid bombardment. *Icarus* **132**, 1–35.

Cuzzi, J. N., R. G. French, L. Dones, P. R. Estrada, and M. R. Showalter 2000. Multicolor photometry of Saturn's main rings from HST and Voyager: Color variation with phase, opening angle, location, and optical depth. *Bull. Am. Astron. Soc.* **32**, 1087.

Cuzzi, J. N., R. G. French, and L. Dones 2002. HST multicolor (255–1042 nm) photometry of Saturn's main rings. I. Radial profiles, phase and opening angle variations, and regional spectra. *Icarus* **158**, 199–223.

Davis, J. N., N. McBride, S. L. Ellison, S. F. Green, and D. R. Ballantyne 1998. Visible and infrared photometry of six Centaurs. *Icarus* **134**, 213–227.

Epstein, M. A. Janssen, and J. N. Cuzzi 1984. Saturn's rings: 3-mm low-inclination observations and derived properties. *Icarus* **58**, 403–411.

Grundy, W., and B. Schmitt 1998. The temperature-dependent near-infrared absorption spectrum of hexagonal H_2O ice. *J. Geophys. Res.* **103**, 25,809–25,822.

Grundy, W. M., M. W. Buie, J. A. Stansberry, J. R. Spencer, and B. Schmitt 1999. Near-infrared spectra of icy outer Solar System surfaces: Remote determination of H_2O ice temperatures. *Icarus* **142**, 536–549.

Hapke, B. 1993. *Theory of Reflectance and Emittance Spectroscopy.* Cambridge Univ. Press, Cambridge, UK.

Hudgins, D. M., S. A. Sandford, L. J. Allamandola, and A. G. Tielens 1993. Mid- and far-infrared spectroscopy of ices—Optical constants and integrated absorbances. *Astrophys. J. Suppl. Ser.* **86**, 713–870.

Jewitt, D., J. Luu, and C. Trujillo 2000. Colors of Kuiper Belt objects from Keck and Subaru. *Bull. Am. Astron. Soc.* **32**, 1029.

Karkoschka, E. 1994. Spectrophotometry of the jovian planets and Titan at 300- to 1000-nm wavelength: The methane spectrum. *Icarus* **111**, 174–192.

Khare, B. N., C. Sagan, E. T. Arakawa, F. Suits, T. A. Callcott, and M. W. Williams 1984. Optical constants of organic tholens produced in a simulated titanian atmosphere: From soft X-ray to microwave frequencies. *Icarus* **60**, 127–134.

Lebofsky, L. A., and M. B. Fegley Jr. 1976. Chemical composition of icy satellites and Saturn's rings. *Icarus* **28**, 379–388.

McCord, T. B., and 11 colleagues 1997. Organics and other molecules in the surfaces of Callisto and Ganymede. *Science* **278**, 271–275.

Mennella, V., J. R. Brucato, L. Colangeli, P. Palumbo, A. Rotundi, and E. Bussoletti 1998. Temperature dependence of the absorption coefficient of cosmic analog grains in the wavelength range 20 microns to 2 millimeters. *Astrophys. J.* **496**, 1058–1066.

Molina, A., F. Moreno, M. Kidger, and J. L. Ortiz 1995. Near-infrared CVF spectrophotometry of Saturn in 1992. *Astron. Astrophys.* **268**, 624–627.

Mukai, T., and C. Koike 1990. Optical constants of olivine particles between wavelengths of 7 and 200 microns. *Icarus* **87**, 180–187.

Owen, T. B., D. P. Cruikshank, C. M. Dale Ore, T. R. Geballe, T. L. Roush, C. de Bergh, R. Meier, Y. J. Pendleton, and B. N. Khare 2001. Decoding the domino: The dark side of Iapetus. *Icarus* **149**, 160–172.

Pilcher, C. B., C. R. Chapman, L. A. Lebofsky, and H. H. Kieffer 1970. Saturn's rings: Identification of water ice. *Science* **167**, 1372–1373.

Pollack, J. B., A. Summers, and B. Baldwin 1973. Estimates of the size of the particles in the rings of Saturn and their cosmogonic implications. *Icarus* **20**, 263–278.

Pollack, J. B., D. Hollenbach, S. Beckwith, D. P. Simonelli, T. Roush, and F. Wesley 1994. Composition and radiative properties of grains in molecular clouds and accretion disks. *Astrophys. J.* **421**, 615–639.

Poulet, F., E. Karkoschka, and B. Sicardy 1999. Spectrophotometry of Saturn's small satellites and rings from Hubble Space Telescope images. *J. Geophys. Res.* **104**, 24,095–24,110.

Poulet, F., J. N. Cuzzi, R. G, French, and L. Dones 2002a. A study of Saturn's ring phase curves from HST observations. *Icarus* **158**, 224–248.

Poulet, F., J. N. Cuzzi, D. P. Cruikshank, T. Roush, and C. Dalle Ore 2002b. Comparison between the Shkuratov and Hapke theory scattering theories for solid planetary surfaces. Applications to the surface composition of two Centaurs. *Icarus*, in press.

Puetter, R. C., and R. W. Russel 1977. The 2–4 μm spectrum of Saturn's rings. *Icarus* **32**, 37–40.

Rouleau, F., and P. G. Martin 1991. Shape and clustering effects on the optical properties of amorphous carbon. *Astrophys. J.* **377**, 526–540.

Shkuratov, Y., L. Starukhina, H. Hoffmann, and G. Arnold 1999. A model of spectral albedo of particulate surfaces: Implications for optical properties of the Moon. *Icarus* **137**, 235–246.

Thompson, W. R., S. K. Singh, B. N. Khare, and C. Sagan 1989. Triton: Stratospheric molecules and organics sediments. *Geophys. Res. Lett.* **16**, 981–984.

Warren, S. G. 1984. Optical constants of ice from the ultraviolet to the microwave. *Appl. Opt.* **23**, 1206–1225.